

REVIEW

View Article Online
View Journal | View IssueCite this: *Mater. Chem. Front.*,
2026, 10, 522

Recent advances in room-temperature phosphorescence metal–organic frameworks: structural design, property modulation, and emerging applications

Xiaoya Bi,^{ab} Yu Xiong *^a and Ben Zhong Tang ^c

Room-temperature phosphorescence (RTP) has attractive features of large Stokes shifts, long-lived emission, and diverse excited-state manifolds, yet its advancement is limited by the stringent requirements of efficient generation and robust stabilization of triplet excitons. Metal–organic frameworks (MOFs) present a particularly elegant platform to overcome this limitation: metal nodes/clusters act as internal heavy atoms to enhance spin–orbit coupling, thereby promoting intersystem crossing, while the rigid, porous architecture of the MOFs facilitates the immobilization of phosphors to suppress non-radiative decay and enables the construction of a protective microenvironment that excludes molecular oxygen. This review provides a timely and systematic overview of the advances in MOF-based RTP systems over the past three years. We categorize the structural design strategies into two archetypes: phosphorescent ligands as structural motifs and a host–guest approach. A detailed discussion further elucidates how metal-node species, ligand engineering, guest/solvent environments, and external stimulus modulate the RTP performance. Emerging applications in solid-state lighting, chemical sensing, anti-counterfeiting, and high-security information encryption are also examined. Finally, current challenges and future directions are outlined to guide the rational design of high-performance MOF-based RTP materials.

Received 30th October 2025,
Accepted 10th December 2025

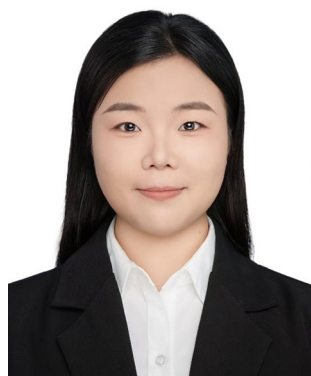
DOI: 10.1039/d5qm00773a

rsc.li/frontiers-materials

^a Center for AIE Research, Shenzhen Key Laboratory of Polymer Science and Technology, Guangdong Research Center for Interfacial Engineering of Functional Materials, College of Materials Science and Engineering, Shenzhen University, Shenzhen, 518061, China. E-mail: xiongyu@szu.edu.cn

^b College of Physics and Optoelectronic Engineering, Shenzhen University, Shenzhen, 518060, China

^c School of Science and Engineering, Shenzhen Institute of Aggregate Science and Technology, The Chinese University of Hong Kong, Shenzhen (CUHK-Shenzhen), Shenzhen, 518172, China



Xiaoya Bi

Xiaoya Bi is a postdoctoral fellow at the Shenzhen University. She received her PhD from Jiangsu University in 2024. Her research interests include the design, construction and application of room-temperature phosphorescent materials based on metal–organic frameworks.



Yu Xiong

Yu Xiong received his PhD in Chemistry and Physics of Polymers from the Shanghai Institute of Organic Chemistry, Chinese Academy of Sciences, and conducted postdoctoral research at the HKUST Shenzhen Research Institute under the supervision of Prof Ben Zhong Tang. She is currently an Associate Professor in College of Materials Science and Engineering of Shenzhen University, focusing on the research studies of organic room-temperature phosphorescence and aggregation-induced emission materials.

1. Introduction

Room-temperature phosphorescence (RTP) is a distinctive photophysical phenomenon characterized by long-lived luminescence that persists from seconds to hours under ambient conditions.¹ Owing to its large Stokes shift, prolonged emission lifetime, and inherent time-gated capability—which collectively enable effective elimination of background fluorescence interference—RTP has attracted intense interest for advanced applications such as anti-counterfeiting,² information encryption,³ chemical sensing,⁴ and bioimaging.⁵ Phosphorescence arises from slow radiative transition from the triplet excited state (T_1) to the singlet ground state (S_0). Therefore, the rational design of efficient RTP systems must address two pivotal issues: (1) enhancing intersystem crossing (ISC) by strengthening spin-orbit coupling (SOC) and/or reducing the singlet–triplet energy gap (ΔE_{ST}). This can be achieved through the incorporation of heavy atoms (e.g., Cl and Br)^{6,7} or heteroatoms bearing lone-pair electrons (e.g., N, O, and S),^{8–10} or by constructing charge-transfer donor–acceptor (D–A) architectures;¹¹ and (2) stabilizing the generated triplet excitons by suppressing nonradiative molecular motions and shielding them from molecular oxygen, which is achievable *via* crystal engineering¹² or confining phosphors within rigid hosts such as polymeric matrices¹³ or porous organic frameworks.¹⁴ Simultaneously satisfying these two requirements remains a big challenge in developing high-performance RTP materials, underscoring the need for innovative material platforms to overcome this hurdle.

Metal–organic frameworks (MOFs) are crystalline porous architectures formed by coordination-driven self-assembly of metal nodes/clusters with organic linkers.¹⁵ Their intrinsic long-range order, programmable topology, and permanent porosity collectively satisfy the two above-mentioned prerequisites for efficient RTP: the generation and stabilization of triplet excitons.^{16,17} First, metal nodes, particularly closed-shell d^{10} ions such as Zn^{2+} and Cd^{2+} , act as heavy-atom perturbators that can enhance SOC, thereby accelerating the ISC process and



Ben Zhong Tang

Ben Zhong Tang is the Dean and Presidential Chair Professor at the School of Science and Engineering, The Chinese University of Hong Kong, Shenzhen. He received his PhD from Kyoto University and is an Academician of the Chinese Academy of Sciences. Professor Tang coined the concept of aggregation-induced emission (AIE) in 2001. His research interests include the exploration of new advanced materials, new luminescence processes, and new polymerization.

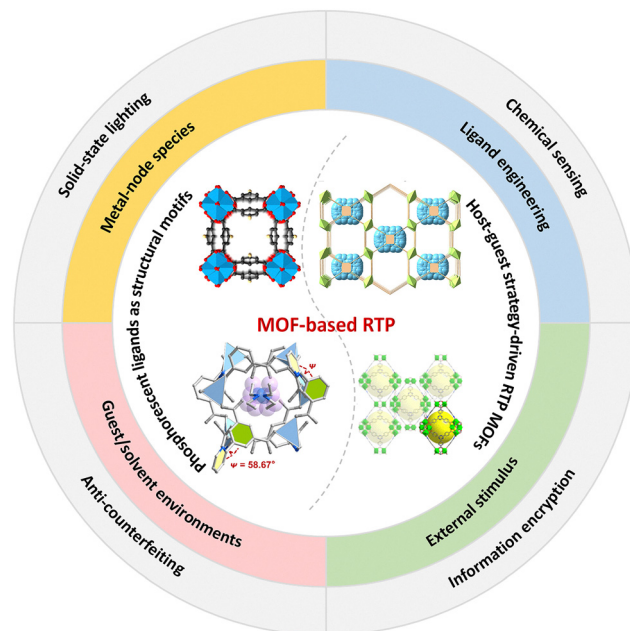


Fig. 1 Schematic illustration of MOF-based RTP materials: (i) structural design strategies—phosphorescent ligands as structural motifs and the host–guest approach; (ii) regulation strategies—metal-node species, ligand engineering, guest/solvent environments, and external stimulus; and (iii) emerging applications—solid-state lighting, chemical sensing, anti-counterfeiting, and high-security information encryption. Reproduced from ref. 30 with permission from Wiley-VCH GmbH, copyright 2025. Reproduced from ref. 31 with permission from Wiley-VCH GmbH, copyright 2025. Reproduced from ref. 32 with permission from American Chemical Society, copyright 2023. Part of this figure has been published in *CCS Chemistry* (2025); ‘Donor–Acceptor Metal–Organic Frameworks Featuring Tunable Triplet States for Multistimulus Responsive Room-Temperature Charge Transfer Phosphorescence’ is available online at <https://doi.org/10.31635/ccschem.024.202404116>. Reproduced with permission.

promoting triplet exciton formation.¹⁸ Second, the rigid framework of MOFs can effectively immobilize chromophores, thereby suppressing nonradiative decay pathways.¹⁹ Third, the programmable pore size enables spatial isolation of emitters from common environmental quenchers such as molecular oxygen and water, while simultaneously accommodating guest sensitizers/emitters to build cascaded energy- or electron-transfer pathways.^{20,21} Leveraging these advantages, MOF-based RTP systems have made rapid strides in recent years, delivering quantum-yield-enhanced emitters,²² multicolor (including white-light) phosphors,^{23,24} ultralong-afterglow materials,²⁵ and stimuli-responsive phosphorescence triggered by humidity,²¹ pressure,²⁶ acid and base vapors,²⁷ and light irradiation.²⁸ Compared with other crystalline porous materials (e.g., covalent organic frameworks and hydrogen-bonded organic frameworks), MOFs offer superior tunability through metal-specific SOC modulation, distinctive cluster-based photophysics, and modular chemistry that readily accommodates host–guest confinement and defect engineering (e.g., missing-linker or linker halogenation), enabling precise control over triplet generation, migration, and protection.^{17,34–36}

Consequently, MOF-based RTP has emerged as a versatile platform for advanced applications in solid-state lighting, high-sensitivity sensing, and next-generation anti-counterfeiting technologies.

Notwithstanding rapid advances in MOF-based RTP materials, systematic and in-depth reviews remain limited. An early survey³⁷ on long-afterglow MOFs offered a preliminary overview of RTP mechanisms and applications, but its scope was inevitably constrained by the developmental stage of the field at that time. More recent overviews focusing on metal–organic hybrids^{29,38} or crystalline porous organic frameworks^{39,40} have only touched on the phosphorescence properties of MOFs, without in-depth analysis of their structural design and the dynamic modulation of structure–property correlations. To address this gap, this review highlights the latest advances in MOF-based RTP materials from 2023 to present, integrating contemporary design principles with performance-modulation strategies to advance the field (Fig. 1). We meticulously elucidate how metal-node species, ligand engineering, guest/solvent environments, and external stimulus govern phosphorescence efficiency through enhanced SOC, optimized electronic structures, and tailored framework topology, thereby establishing clear structure–emission relationships. These insights are then connected to transformative applications in solid-state lighting, chemical sensing, anti-counterfeiting, and information encryption. Finally, we outline the key challenges and emerging opportunities and propose mechanism-grounded guidelines to steer the rational design of next-generation high-performance MOF-based RTP materials.

2. Strategies of structural design

In the domain of MOF-based RTP materials, structural design constitutes a governing factor for achieving high-performance phosphorescent outputs. The fundamental objective centers on orchestrating excitonic environments that concurrently: (i) promote efficient ISC and (ii) suppress non-radiative decay channels. Two dominant paradigms emerge to realize these criteria: intrinsically phosphorescent motifs constituting structural frameworks and host–guest confinement strategies

activating phosphorescence (Fig. 2). These orthogonal yet complementary strategies—distinct in their mechanistic underpinnings but unified in harnessing crystalline rigidity—provide versatile avenues to engineer triplet population dynamics and emission properties in MOF architectures, as detailed in the following subsections.

2.1. Phosphorescent ligands as structural motifs

The common and effective strategy for constructing MOF-based RTP materials involves the direct coordination of intrinsically phosphorescent ligands to metal centers. This approach leverages the ordered rigidity of MOF frameworks for site-selective immobilization while enabling precise modulation of electronic coupling and intersystem crossing (ISC) pathways through tailored metal coordination.^{19,41,42} Commonly employed ligands include nitrogen or/and oxygen heteroatoms (*e.g.*, aromatic carboxylic acids, and nitrogen-containing heterocycles, Fig. 3A).^{16,41–46} Their $n\text{-}\pi^*$ transitions and tunable D–A characteristics accelerate SOC or reduce ΔE_{ST} to enhance ISC efficiency.^{20,47,48} Furthermore, the electronic structure and coordination geometry of metal nodes can critically modulate the SOC intensity and metal–ligand charge transfer (MLCT/LMCT) involvement, thereby establishing an optimal balance between ISC enhancement and preservation of ligand-centered emission.

In 2024, Long *et al.*⁴⁵ reported a Ca-MOF (CaL-3) assembled from 2,3-pyrazinedicarboxylic acid (H_2PZDC) and $\text{Ca}(\text{NO}_3)_2 \cdot 4\text{H}_2\text{O}$ that exhibited orange RTP with emission maxima at 564 nm (298 K) and 556 nm (77 K), an ultralong phosphorescence lifetime (τ_{p}) of 521 ms at room temperature, and a visible afterglow of about 5 s. The persistent luminescence was attributed to two synergistic factors: enhanced SOC *via* lone-pair electrons of O/N atoms in H_2PZDC under the El-Sayed rule; and rigidification-induced suppression of nonradiative decay through coordination, intramolecular hydrogen bonding, and dense packing. Critically, coordination to Ca^{2+} increased the phosphorescence intensity by roughly an order of magnitude relative to the free ligand, illustrating metal-directed amplification. Furthermore, coordination bond length directly governs phosphorescence performance in ligand-centered MOF systems

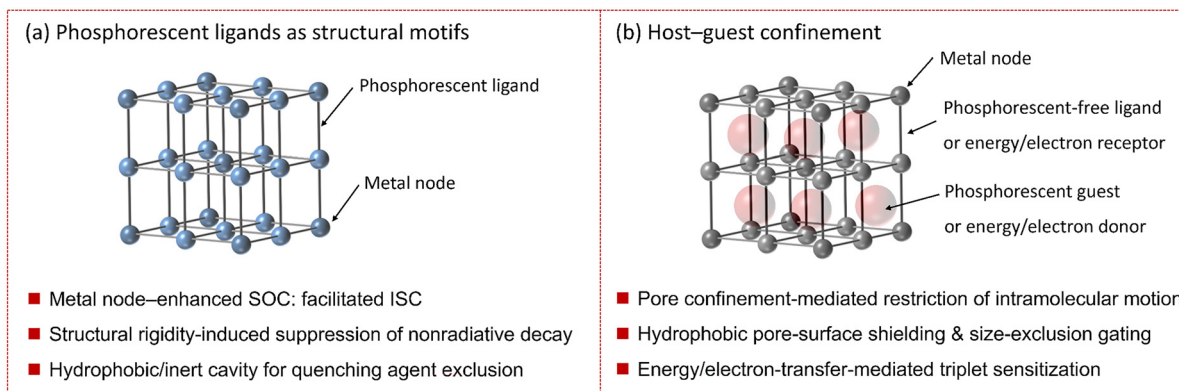


Fig. 2 Schematic of two MOF-based RTP structural strategies: (a) phosphorescent ligands as structural motifs and (b) host–guest confinement.

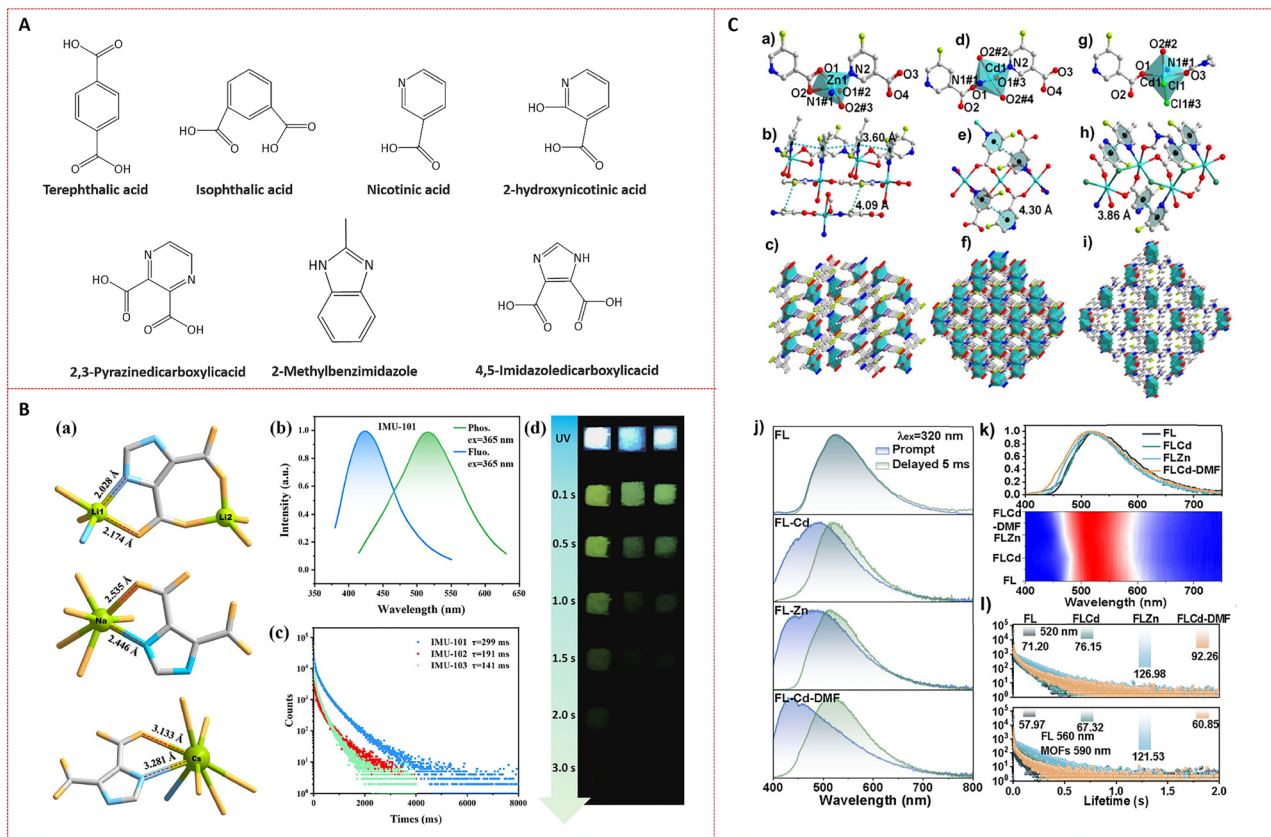


Fig. 3 (A) Common phosphorescent ligands. (B) The structure and photophysical properties of base metal-based MOFs: (a) minimum asymmetric coordination unit of IMU-101, IMU-102, and IMU-103; (b) photoluminescence emission spectra of IMU-101; (c) phosphorescence decay curves of IMU-101, IMU-102, and IMU-103 at room temperature; (d) crystal photographs of IMU-101, IMU-102, and IMU-103 during and after irradiation by 365 nm UV light, respectively. Reproduced from ref. 49 with permission from Springer Nature, copyright 2025. (C) The structure and photophysical properties of FLZn, FLCd, and FLCd-DMF: (a), (d) and (g) asymmetric units of FLZn, FLCd, and FLCd-DMF. (b), (e) and (h) π - π stacking interactions within FLZn, FLCd and FLCd-DMF, respectively; (c), (f) and (i) 3D supramolecular structures of three MOFs; (j) prompt and delayed spectra of FL, FLCd, FLZn, and FLCd-DMF; (k) superimposed and normalized delayed spectra of FL and three MOFs; (l) phosphorescence lifetimes of FL, FLCd, FLZn, and FLCd-DMF. Reproduced from ref. 50 with permission from American Chemical Society, copyright 2025.

by modulating the crystallographic structure. Ma *et al.*⁴⁹ synthesized an alkali-metal series of MOFs (IMU-101, IMU-102, and IMU-103; IMU = Inner Mongolia University, Fig. 3B) using the 4,5-imidazoledicarboxylate ligand. IMU-101 (Li) delivered the best performance, with a 525 nm phosphorescence lifetime of 299 ms—exceeding IMU-102 (191 ms) and IMU-103 (141 ms)—and an afterglow discernible for 3 s. Crystallography and density functional theory (DFT) calculations indicated that ultra-short Li-N/O bonds (1.850–2.172 Å) compacted the lattice and rigidified the chromophore environment, lowering k_{nr} and enabling efficient RTP without heavy atoms. In parallel, Chen *et al.*⁵⁰ employed the rigid and halogenated ligand 5-fluoronicotinic acid (FL) to self-assemble three excitation-dependent long-afterglow MOFs with ZnCl_2 or CdCl_2 (FLCd, FLZn, and FLCd-DMF, Fig. 3C). These materials displayed prompt and delayed emissions tunable from blue/cyan to green and produced cool-white output under specific excitation (340 nm for FLCd/FLZn; 280 nm for FLCd-DMF), with afterglow modulated by the excitation wavelength and temperature. Integrated crystallographic, photophysical, and computational

analyses showed that multicolor afterglow arose from concurrent ligand-centered and aggregation-induced triplet emissions, whereas phosphorescence enhancement stemmed from the combined effects of heavy-atom perturbation (Cd and F/Cl), coordination-enforced interlocking, and dense supramolecular constraints (π - π stacking, C-H...O/F hydrogen bonding, halogen bonding). Notably, despite a calculated increase in SOC along $\text{FL} < \text{FLZn} < \text{FLCd} < \text{FLCd-DMF}$, FLZn exhibited the longest lifetimes, underscoring the primacy of packing induced rigidification and oxygen management over SOC alone. Leveraging these tunable afterglow features, the authors demonstrated time-encoded information encryption/decryption.

2.2. Host-guest approach

MOFs provide an ideal host platform for guest-derived RTP by integrating three critical functions: (1) confinement-engineered exciton management through high-surface-area nanocavities that enforce spatial isolation of phosphors—suppressing triplet-triplet annihilation while restricting intramolecular motions to minimize non-radiative decay;^{24,51,52}

(2) oxygen/water exclusion *via* hydrophobic pore walls or size-selective apertures that physically block molecular oxygen and moisture;⁵³ and (3) programmable energy cascades enabled by crystalline-directed host-guest alignment, facilitating energy/electron-transfer-mediated triplet sensitization.^{21,54,55} These attributes collectively address the core challenges of RTP—enhancing ISC efficiency, extending triplet lifetimes, and directing exciton migration—while enabling atomic-level structure-property correlations.

Recent advances have converged on two dominant host-guest design paradigms for MOF-based RTP systems: the first leverages nanoconfinement of phosphorescent guests within precisely engineered framework cavities to promote confinement-driven triplet generation and protection.⁵⁶ A representative example was a lutetium-based framework (Lu-MOF) that employed formic acid as the sole linker and furnished 1D channels for dye confinement.⁵⁷ Encapsulating 4,4'-bipyridine in these channels could activate its phosphorescence (no phosphorescence in the solid or in formamide). Under 365 nm excitation, the composite showed blue fluorescence at 435 nm (Fig. 4A). After the excitation was turned off, it produced a broad green afterglow centered at 545 nm, with a phosphorescence lifetime of 110.1 ms and a naked-eye

persistence of 0.7 s. Mechanistically, the rigid, spatially confining channels suppressed molecular rotations and vibrations, reduced nonradiative loss, enabled ISC, and stabilized triplet decay. Moreover, partial substitution of Lu³⁺ with Eu³⁺ modulated the emission color and established graded control over afterglow intensity, thereby providing a route to multilevel, time-encoded optical outputs. Beyond spatial confinement, MOF hosts can also amplify triplet populations in guest phosphors through sensitization mechanisms: framework-generated triplets (or those from co-encapsulated sensitizers) undergo ISC, and then transfer to guests *via* triplet-triplet energy transfer (TTET), thereby enhancing RTP efficiency. Zhang *et al.*³¹ engineered chiral MOFs (DCF-12 and LCF-12) as host matrices for pyrene-derived phosphors, revealing that the T₁ state of the TPE ligand occupies an intermediate energy position between the S₁ and T₁ states of guests DMP and R/S-PEPCA. This strategic energetic alignment enables the TPE ligand to mediate cascade energy transfer: energy migrates from the S₁ state of DMP and R/S-PEPCA to the T₁ state of TPE, followed by subsequent transfer to the T₁ states of the guest phosphors. This sequential energy relay effectively reduces ΔE_{ST} , thereby facilitating the ISC process and enhancing RTP behavior (Fig. 4B).

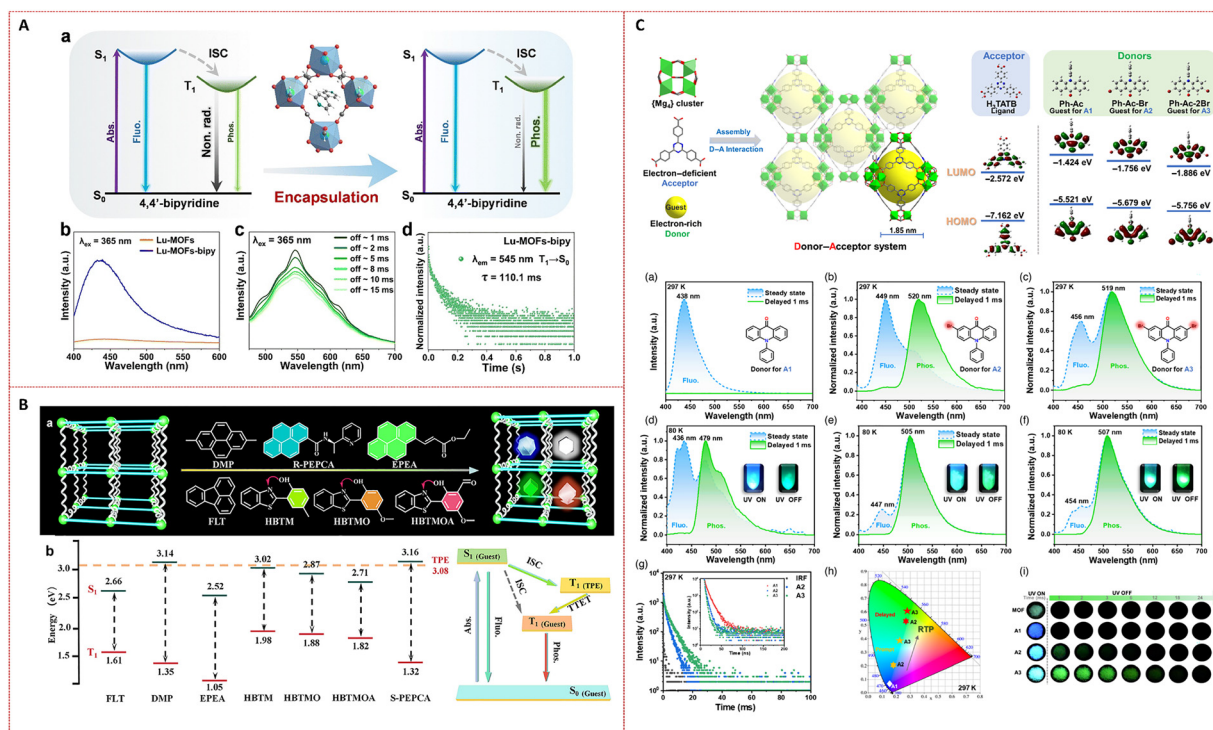


Fig. 4 (A) The RTP mechanism and photophysical properties of Lu-MOFs-bipy: (a) the schematic illustration of Lu-MOFs-bipy green RTP mechanism; (b) the fluorescence spectra of Lu-MOFs and Lu-MOFs-bipy in the solid state; (c) the RTP spectra of Lu-MOFs-bipy; (d) decay curve of the phosphorescence monitored at 545 nm for Lu-MOFs-bipy. Reproduced from ref. 57 with permission from the Royal Society of Chemistry, copyright 2025. (B) Schematic illustration of (a) encapsulation of guest molecules into chiral MOFs and (b) energy levels of guest and ligand molecules. Reproduced from ref. 31 with permission from Wiley-VCH GmbH, copyright 2025. (C) Composition and photophysical properties of the D-A MOF system: steady state and delayed spectra of A1, A2, and A3 at (a)–(c) room temperature and (d)–(f) 80 K; (g) Lifetime decay curves, (h) CIE coordinate, and (i) luminescence photographs of A1–A3. Part of this figure has been published in *CCS Chemistry* (2025); 'Donor-Acceptor Metal-Organic Frameworks Featuring Tunable Triplet States for Multistimulus Responsive Room-Temperature Charge Transfer Phosphorescence' is available online at <https://doi.org/10.31635/ccschem.024.202404116>. Reproduced with permission.

In addition to spatially confining phosphorescent guests, RTP can be activated by engineering D–A channels that mediate charge and triplet energy transfer between MOFs and guests.²¹ A seminal study by Geng *et al.*³³ demonstrated an Mg-based donor–acceptor platform using the electron-deficient triazine carboxylate linker H₃TATB as the acceptor and encapsulating electron-rich acridone derivatives—10-phenyl-9(10*H*)-acridone (Ph-Ac), 2-bromo-10-phenyl-9(10*H*)-acridone (Ph-Ac-Br), and 2,7-bromo-10-phenyl-9(10*H*)-acridone (Ph-Ac-2Br)—*via* solvo-thermal synthesis to generate D–A composites A1–A3 (Fig. 4C). Through-space charge transfer (TSCT) between the host NKU-Mg-2 and guest molecules narrowed ΔE_{ST} , thereby facilitating ISC and enabling tunable RTP. Specifically, A1 (Ph-Ac@NKU-Mg-2) exhibited solely fluorescence at 438 nm at room temperature, with phosphorescence emerging at 479 nm only under cryogenic conditions (80 K); A2 (Ph-Ac-Br@NKU-Mg-2) displayed dual room-temperature emission (fluorescence: 449 nm; RTP: 520 nm, $\tau_p = 1.60$ ms); and A3 (Ph-Ac-2Br@NKU-Mg-2) delivered further enhanced RTP ($\tau_p = 3.35$ ms), attributed to heavy-atom-induced SOC amplification and increased ISC efficiency. The platform also exhibits responsiveness to multiple stimuli (X-rays, temperature, and oxygen), underscoring MOF-programmed TSCT and SOC engineering as a precise strategy for triplet-state manipulation in RTP materials.

3. Regulation of RTP properties

The phosphorescence performance of MOF-based RTP materials is governed by three intrinsically coupled elements:^{48,58–61} (i) metal nodes/clusters dictating coordination geometry, electronic coupling, and MLCT/LMCT pathways; (ii) organic linkers encoding excited-state landscapes through conjugation, heteroatom integration, and rigidity; and (iii) guest/solvent environments modulating microenvironmental polarity and rigidity,

oxygen permeability, and energy/electron transfer processes. Complementing these intrinsic elements, external stimuli (*e.g.*, pressure and temperature) serve as a dynamic fourth dimension to reconfigure triplet energy-level alignment, modulate exciton migration rates, and suppress non-radiative decay pathways. This synergistic quadripartite framework enables precise tuning of emission color, lifetime, photoluminescence quantum yield (Φ_{PL}), and afterglow duration while imparting multifunctionality (Table 1).

3.1. Metal-node species

The electronic structure and ligand-field environment of metal nodes critically determine the SOC strength and the degree of MLCT/LMCT, thereby governing key RTP parameters, including the ISC rate constant (k_{ISC}), ΔE_{ST} , emission color, and lifetime.²⁹ Rational variation of the metal identity, coordination number, and coordination geometry provides a direct handle to modulate RTP performance. Among available metal nodes, closed-shell d¹⁰ ions (*e.g.*, Zn²⁺ and Cd²⁺) have been favored as photophysically “inert” scaffolds that support ligand-centered emission: their fully occupied d manifolds suppress quenching *via* d–d transitions, while the internal heavy-atom effect enhances SOC and promotes ISC.²³ As a representative example, Zhang *et al.*⁶² synthesized Zn-binc and Cd-binc MOFs using 2-(1*H*-benzimidazol-1-yl)nicotinic acid (Hbinc) *via* site-selective coordination. Zn²⁺ coordinated to three Hbinc sites (imidazole N, pyridyl N, and carboxylate O) and Cl[−] to form a 2D layered network with bimodal porosity, whereas Cd²⁺ bound two Hbinc sites, generating a 1D chain; both architectures further assembled through intermolecular hydrogen bonding. The distinct coordination preferences dictated Hbinc torsion angles and packing density, thereby promoting ISC and suppressing nonradiative decay. Crucially, Cd-binc exhibited a smaller ΔE_{ST} value than Zn-binc, affording a longer RTP lifetime (188 ms at 534 nm *versus* 123 ms at 541 nm) and a shorter

Table 1 Photophysical properties of representative MOF-based RTP materials

Modulation mode	Modulation strategies	MOF designation (as reported)	λ_p (nm)	Φ_{PL} (%)	Φ_p (%)	τ_p (ms)	Ref.
Metal-node	Metal identity	Zn-binc	541			123	62
		Cd-binc	534			188	
	Metal precursor	LIFM-130	485	36		93	63
		LIFM-131	490	16		47	
		LIFM-132	480	24		22	
Ligand	Ligand modification	CAU-10-H	495	25.2		638	64
		CAU-10-CH ₃	507	7.7		101	
		CAU10-OCH ₃	536	4.4		1.5	
	Mixed-ligand	MOF-a	548	28.7		188	68
		MOF-b	588	24.9		1.1	
Guest	Solvent-induced polymorphism	1	485	11.94		264.6	70
		2	495	5.77		0.083	
	Solvent-guest-mediated microenvironment tuning	IMOF-DMF	500	12.27		206	71
		IMOF-DEF	514	1.76		173	
Other	Solvent stimulation	Eu-BPIPA2 ⊂ CB[8]	500	5.34	2.79	1.01	72
		Eu-BPIPA2 ⊂ CB[8]/MeOH	500	10.20	1.26	0.603	
	Thermal stimulation	LIFM-SHL-3b	572	8	1.7	0.01	73
		LIFM-SHL-3c	594	7.5	2.5	0.47	

λ_p : phosphorescence emission wavelength; Φ_{PL} : photoluminescence quantum yield; Φ_p : phosphorescence quantum yield; and τ_p : phosphorescence lifetime.

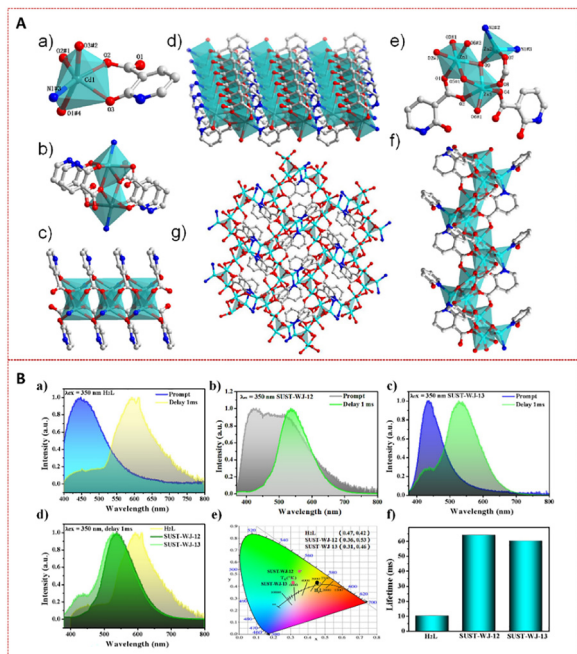


Fig. 5 (A) Crystal structures of SUST-WJ-12 and SUST-WJ-13: asymmetric units and coordination environments of (a) Cd and (e) Zn ions; (b) dinuclear Cd cluster and (c) metal ribbon in SUST-WJ-12; self-assembly formed the 2D framework structure of (d) SUST-WJ-12 and (g) SUST-WJ-13; (f) 1D metal chain in SUST-WJ-13. (B) RTP properties of H₂L, SUST-WJ-12 and SUST-WJ-13: prompt and delayed spectra of (a) H₂L, (b) SUST-WJ-12, and (c) SUST-WJ-13; (d) superposition of delayed spectra, (e) CIE coordinates, and (f) the lifetimes. Reproduced from ref. 44 with permission from Elsevier, copyright 2023.

fluorescence lifetime, demonstrating metal-dependent control over triplet-state dynamics.

Transitioning from mononuclear nodes to multinuclear clusters can afford greater leverage over RTP regulation in MOFs by simultaneously rigidifying ligand conformations and amplifying SOC. Wang *et al.*⁴⁴ engineered two cluster-based MOFs—SUST-WJ-12 (Cd₂ binuclear clusters, Fig. 5A) and SUST-WJ-13 (Zn₃ trinuclear clusters)—assembled with 2-hydroxynicotinic acid (H₂L). Both architectures exhibited excitation-dependent blue-to-green chromatic tuning and room-temperature RTP with lifetimes of 69.92 and 63.22 ms, respectively, together with bright long-persistent luminescence visible for 2–3 s after cessation of UV irradiation (Fig. 5B). Steady-state/delayed spectra and theoretical calculation analyses confirmed ligand-centered emissions while revealing cluster-mediated SOC enhancement at metal–ligand interfaces. Synergistic contributions from cluster nuclearity and hydrogen-bonded dense packing collectively stabilized triplet excitons and reduced ΔE_{ST} , enabling programmable afterglow color modulation.

Moreover, anions from metal salt precursors critically tune MOF phosphorescence by entering the coordination sphere as terminal or bridging ligands to form metal-halide clusters. Mo *et al.*⁶³ demonstrated this by constructing three MOFs from identical ligands but different metal salts: LIFM-130 (CdCl₂), LIFM-131 (Cd(NO₃)₂), and LIFM-132 (Zn(NO₃)₂). LIFM-130

exhibited cyan-to-green emission with the strongest RTP performance: a room-temperature lifetime of 93 ms, a quantum efficiency of 36%, and a bright yellow afterglow persisting 2–3 s post-UV. In contrast, LIFM-131 and LIFM-132 showed blue/cyan emission with shorter lifetimes (47/22 ms) and shorter quantum efficiencies (16%/24%). Periodic DFT analyses attributed the emission primarily to ligand-centered n- π^* (and π - π^*) transitions with MLCT contributions, while only LIFM-130 displayed an additional halogen-to-ligand charge-transfer (CLCT) channel. The coordinated chloride in the Cd–Cl clusters enhanced SOC and compacted the framework *via* stronger noncovalent interactions, rationalizing its superior RTP performance.

3.2. Ligand engineering

Because long persistent luminescence in most MOF-based RTP materials originates from organic ligands, the structural and electronic properties of these organic components play a decisive role in phosphorescence tuning.⁶⁴ Our previous work installed electron-donating groups (–CH₃/–OCH₃) on isophthalic acid (IPA) and achieved lifetime modulation from 6 to 638 ms in heavy-atom-free CAU-10 MOFs (Fig. 6A).³² TD-DFT (time-dependent density functional theory) analyses revealed that electron-donating substitutions redistribute the HOMO electron density from carboxylates to methyl/methoxy groups and the benzene ring, narrowing the S₀–T₁ energy gap and red-shifting the phosphorescence from green to yellow. Similarly, Xue *et al.*⁶⁵ achieved a lifetime enhancement (from 103.94 to 264 ms) with 2 s afterglow in a fluorinated nicotinic acid-based MOF (5FCa-MOF), reinforcing ligand electronic engineering as a general optimization route. Ligand engineering with a D–A topology enables dual phosphorescence in MOFs through concurrent ligand-centered and metal-to-ligand charge transfer (MLCT) emission. Exemplifying this, Wang *et al.*⁶⁶ synthesized a Cu(I) cluster-chain MOF (SUST-WZ3) using the D- π -A- π -D ligand 1,4-bis(4-(1H-tetrazol-5-yl)phenyl)naphthalene (Tz-Nap). The appropriate energy levels of the ligand D- π -A- π -D structure, coupled with Cu-cluster-enhanced SOC and dense packing, promoted efficient ISC while suppressing nonradiative dissipation. This yielded dual emission: near-infrared RTP ($\lambda_{em} = 705$ nm, $\tau_p = 1.85$ ms at 298 K; 25.16 ms at 77 K) and MLCT luminescence (450–505 nm, $\tau_p = 1.07$ –5.38 μ s). Modulating their intensity ratio generated white light, with naked-eye-visible near-infrared afterglow at cryogenic temperatures.

Mixed-ligand strategies expand RTP tunability in MOFs by incorporating secondary organic linkers. Zheng *et al.*⁶⁷ observed in ZnIDC frameworks (assembled from 1H-imidazole-4,5-dicarboxylate and Zn²⁺) that introducing auxiliary ligands 4,4'-bipyridine (bpy) or trans-1,2-bis(4-pyridyl)ethylene (bpe) formed three isostructural compounds, but longer auxiliary ligands sterically blocked hydrogen-bonded energy transfer pathways, reducing afterglow durations from 3 s to less than 0.1 s. Secondary ligands decisively modulate RTP by dictating the orientation and spacing of primary chromophores within MOF frameworks. Using 4'-(4'-(1H-tetrazol-5-yl)-[1,1'-biphenyl]-4-yl)-2,2':6',2''-terpyridine (HTzDTPy) as the

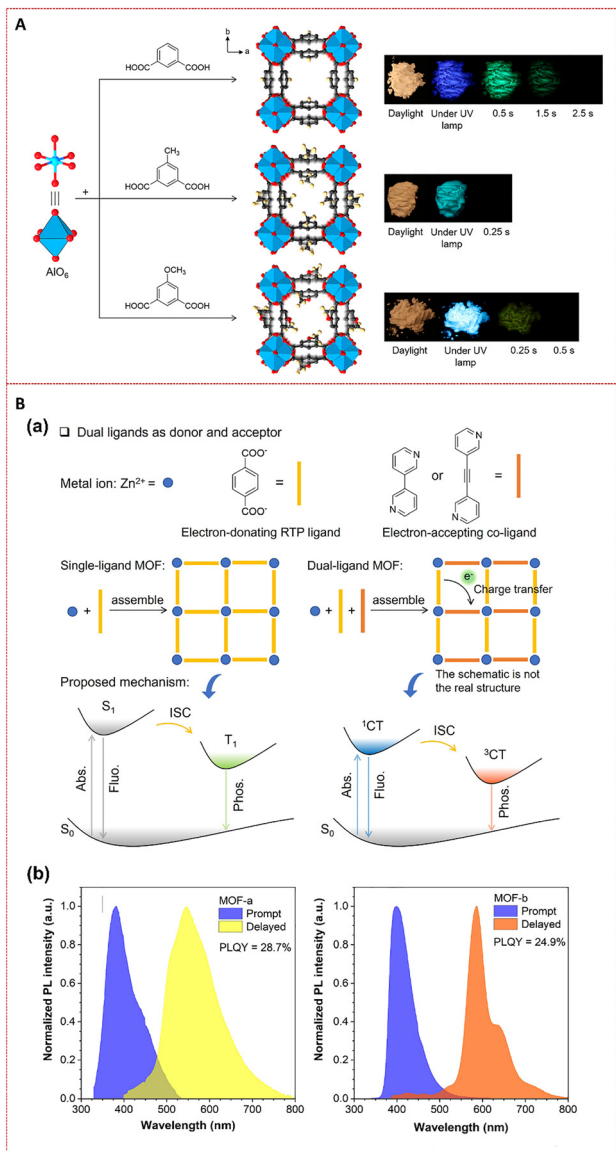


Fig. 6 (A) Schematic diagram of the mechanism for regulating luminescence through ligand functionalization. Reproduced from ref. 32 with permission from American Chemical Society, copyright 2023. (B) Schematic diagram of the mechanism and spectra for achieving redshifted emission by constructing ligand D-A pairs using the mixed-ligand strategy. Reproduced from ref. 68 with permission from American Chemical Society, copyright 2025.

emissive ligand and phthalic acid (PA) or terephthalic acid (TPA) as auxiliary linkers, Mo *et al.* constructed PA-TPY and TPA-TPY.⁶⁹ Both frameworks exhibited red afterglow originating from HTzDTPy after photoexcitation. Crucially, PA enforced a denser packing motif in PA-TPY, extending phosphorescence lifetimes to 10.63 ms at 550 nm and 12.04 ms at 660 nm, in contrast to the shorter lifetimes observed for TPA-TPY. Beyond packing effects, interligand energy/electron transfer in mixed-ligand systems tuned the frontier-orbital energy gaps. In our previous work, an electron-deficient pyridyl secondary ligand was introduced to form robust donor-acceptor

pairs with TPA in a dual-ligand MOF, activating ligand-to-ligand charge transfer (LLCT, Fig. 6B).⁶⁸ The resultant triplet charge-transfer (³CT) state was stabilized below the T1 level of single-ligand MOFs, yielding a bathochromic shift from 510 nm to dual emissions at 548 and 588 nm with lifetimes of 180 ms and 1.1 ms, respectively.

3.3. Guest/solvent environments

Beyond metal nodes and organic linkers, guest species—including residual or coordinating solvents—critically governed RTP by reshaping intermolecular contacts and crystallographic packing. Zhang *et al.*⁷⁰ synthesized two Cd-MOFs, [Cd(L)(DMSO)₂] (1) and [CdL(H₂O)(DMF)_{0.5}(DMSO)_{0.5}]-DMF (2), from 4-(5,7-dioxo-5,7-dihydroimidazo[4,5-*f*])isoindol-6(1*H*)-yl)-benzoic acid using different poly-solvents (DMSO/DMF/EtOH/H₂O for 1; DMSO/DMF/H₂O for 2). Although the metal-ligand composition was identical, the solvent environment imposed distinct packing architectures: 2 adopted an interpenetrated framework with pronounced edge-to-face interactions that stabilized triplet excitons, but simultaneously incorporated high-frequency O-H oscillators (notably coordinated H₂O) that enhanced vibrational quenching. As a result, 2 displayed a lower Φ_{PL} value (5.77% vs. 11.94% for 1) and a dramatically shortened lifetime (83 μs vs. 264.6 ms), highlighting solvent-directed trade-offs between exciton stabilization and nonradiative dissipation.

Even when solvents do not participate in coordination, they can persist as pore guests in MOFs and modulate RTP. Wu *et al.*³⁰ constructed two isorecticular ionic MOFs (IMOF-DMF and IMOF-DEF) by coordinating Zn with 2-(3,5-dicarboxyphenyl)nicotinic acid (H₂L) and leveraging the *in situ* decarbonylation of DMF/DEF. The size disparity between encaged cations ((CH₃)₂NH₂⁺ vs. (CH₃CH₂)₂NH₂⁺) governed pyridyl-ring rotational freedom: the smaller (CH₃)₂NH₂⁺ in IMOF-DMF enforced a larger dihedral angle ($\Psi = 59.88^\circ$) than in IMOF-DEF ($\Psi = 56.99^\circ$), diminishing π -conjugation. This attenuated conjugation synergistically strengthened SOC ($\xi = 2.12 \text{ cm}^{-1}$) while narrowing ΔE_{ST} (0.34 eV), thereby establishing a dual-facilitated ISC mechanism. As a consequence, IMOF-DMF delivered a higher phosphorescence quantum yield (Φ_{p} , 12.27% vs. 1.76% for IMOF-DEF) and a longer lifetime (206 ms at 500 nm vs. 173 ms at 514 nm for IMOF-DEF), accompanied by a bright afterglow visible for approximately 3 s after UV cessation.

Beyond crystallographic packing, solvent guests can also tune the electronic structures of MOFs. Liu *et al.*⁷¹ synthesized two topologically analogous Cd-MOFs (Cd-DMF and Cd-CH₃CN) from Cd²⁺ and 4,5-imidazoledicarboxylic acid, confining DMF or CH₃CN within channels (Fig. 7A). The structurally ordered Cd-CH₃CN exhibited weak green afterglow at 505 nm ($\tau_{\text{p}} = 88.5 \text{ ms}$) from ligand-centered emission. In contrast, guest-induced distortion in Cd-DMF reinforced C-H... π interactions, opening multiple LLCT pathways that populated manifold triplet states.

This produced dual phosphorescence comprising the ligand self-emission at 530 nm ($\tau_{\text{p}} = 196.0 \text{ ms}$; Fig. 7B) and LLCT

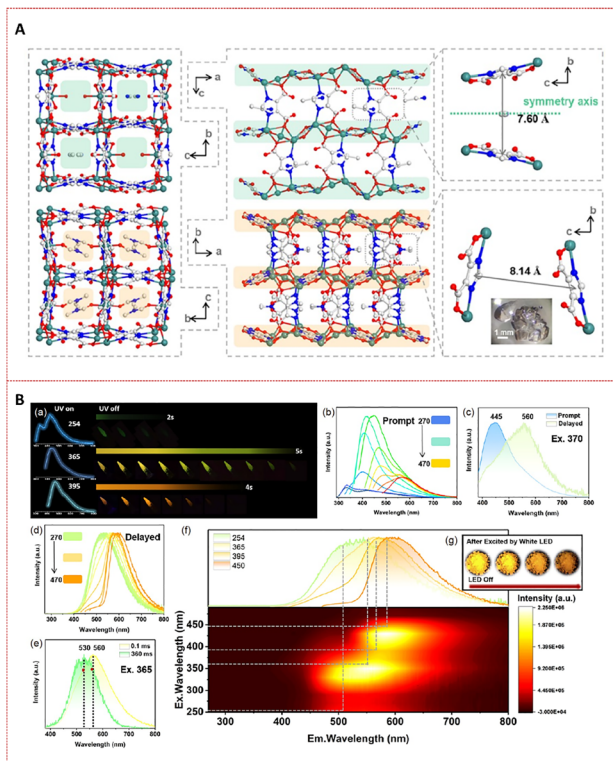


Fig. 7 (A) Structural comparison of Cd-CH₃CN (upper) and Cd-DMF (bottom). (B) Luminous properties of Cd-DMF: (a) emission spectra and corresponding photographs before and after turning off the UV lamp at different excitation wavelengths; (b) prompt spectra at different excitation wavelengths; (c) normalized spectra in prompt and delayed modes; (d) normalized delayed spectra under different excitation wavelengths; (e) normalized RTP emission spectra at different delayed time; (f) phosphorescence-excitation mapping at different excitation wavelengths; (g) photographs taken after turning off a white-light LED lamp. Reproduced from ref. 71 with permission from Springer Nature, copyright 2023.

emission at 560 nm ($\tau_p = 187.0$ ms). The afterglow underwent bathochromic evolution from green to yellow to orange, tunable by the excitation wavelength (270–470 nm) and delay time, and displayed pronounced time-varying afterglow under white-LED excitation.

3.4. External stimulus

Owing to the environmental sensitivity of triplet excitons, the RTP of MOFs can be finely tuned by external stimuli (thermal, mechanical, or chemical). For example, Ni *et al.*⁵⁵ showed that exposure to water switched on green phosphorescence in MOF-5 by transforming it into a denser ZnBDC·xH₂O phase. Water molecules confined in the pores formed extensive hydrogen-bond networks that suppressed ligand vibrations and stabilized triplet states. The authors further exploited this water-induced restructuring as a host-guest doping strategy to create water-activated phosphors (P@ZnBDC·xH₂O). These materials exhibited higher quantum yields than P@MOF-5, emission tunable from green to orange-red, and persistent afterglow lasting 3–6 s. Notably, the lifetime remained 11.37 ms after six weeks of water immersion, enabling aqueous-triggered

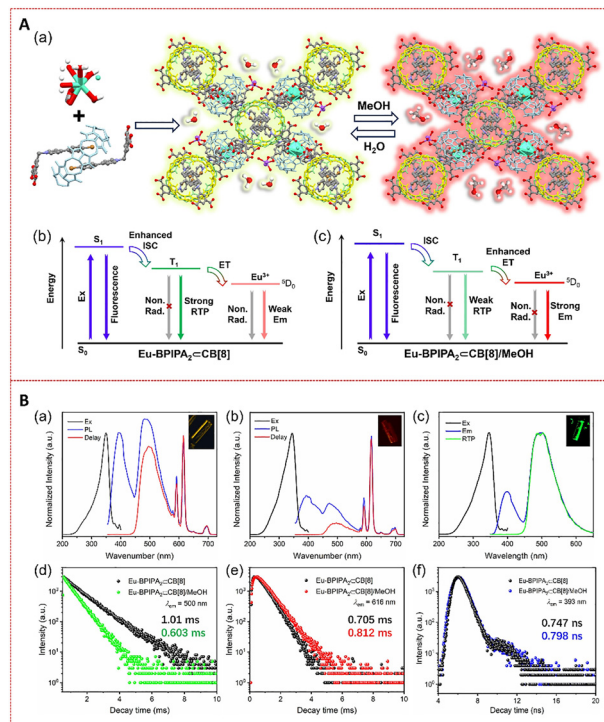


Fig. 8 (A) Schematic diagrams: (a) construction of Ln-MOFs and (b, c) their reversible dynamic switching mechanism between RTP and fluorescence. (B) The photoluminescence behavior of crystals Ln-BPIPA₂@CB[8]: excitation/emission/delayed spectra of (a) Eu-BPIPA₂@CB[8], (b) Eu-BPIPA₂@CB[8]/MeOH and (c) Gd-BPIPA₂@CB[8]; decay curves monitored at (d) 500 nm, (e) 616 nm, and (f) 393 nm of Eu-BPIPA₂@CB[8] and Eu-BPIPA₂@CB[8]/MeOH. Reproduced from ref. 72 with permission from Elsevier, copyright 2025.

information encryption. Similarly, Niu *et al.*⁷² fabricated cucurbit[8]uril (CB[8])-mediated Ln-MOF single crystals by encapsulating an isophthalic acid-functionalized 4-(4-bromophenyl)pyridine salt (H₂BPIPA) in CB[8] cavities, followed by Ln³⁺ coordination (Fig. 8A). In water, only weak electron transfer occurred from the inclusion T₁ to the ⁵D₀ emitting level of the Eu³⁺; in methanol, electron transfer was strengthened and the non-radiative transition of Eu³⁺ was suppressed, enabling reversible switching between RTP and Eu³⁺ emission. Accordingly, Eu-BPIPA₂@CB[8] exhibited intensified green RTP ($\tau_p = 1.01$ ms, $\Phi_p = 2.79\%$) with quenched Eu³⁺ emission, whereas methanol-treated Eu-BPIPA₂@CB[8]/MeOH displayed attenuated RTP ($\tau_p = 0.603$ ms at 500 nm), enhanced Eu³⁺ lifetime at 616 nm (Fig. 8B). These colorless crystals served as stimulus-responsive anti-counterfeiting inks, exhibiting water/methanol-triggered chromism (pale yellow → red) *via* reversible electronic-state modulation. Moreover, temperature stimuli can induce crystal conformational distortions, dynamically modulating phosphorescent properties. Sun *et al.*⁷³ synthesized 4,4'-((2,5-dicyano-1,4-phenylene)bis(sulfanediy))dibenzoic acid (DPSD) with rotatable C–S–C bonds, and then coordinated it with Cd to obtain the stimulus-responsive LIFM-SHL-3a. The torsionally labile C–S–C linkages enabled a temperature-driven conformational rearrangement, yielding reversible

single-crystal-to-single-crystal conversions to LIFM-SHL-3b (350 K) and LIFM-SHL-3c (375 K). This structural dynamism modulated noncovalent interactions and singlet–triplet energy gaps, facilitating a switchable emission mechanism from fluorescence to RTP upon thermal actuation. Mechanical stimuli typically induce crystalline-to-amorphous transitions in MOFs. Sun *et al.*²⁶ prepared a Cd-MOF (LIFM-SHL-2) from 4,4',4'',4'''-(3,6-dicyanobenzene-1,2,4,5-tetrayl)tetrakis(oxy)tetrabenzic acid (DTOT) that displayed multilevel stimulus responsiveness. The LIFM-SHL-2 crystal exhibited green RTP at 298 K ($\lambda_{em} = 498$ nm, $\Phi_{PL} = 2.5\%$) and a markedly enhanced afterglow at 77 K ($\tau_p = 162$ ms). Grinding 5 min triggered amorphization and switched the emission to blue fluorescence (427 nm, $\tau_p = 1.4$ ns). Conversely, DMF immersion or NH_3 exposure restored crystallinity and recovered green RTP with an extended lifetime ($\tau_p = 49.6$ μ s). This reversible switching was attributed to competitive modulation of ΔE_{ST} and nonradiative decay: the crystalline lattice leveraged Cd–O cluster-mediated heavy-atom effects and dense supramolecular interactions to promote ISC and stabilize triplets, whereas amorphization disrupted these pathways, favoring singlet emission.

4. Advanced applications of MOF-based RTP materials

MOF-based RTP materials have emerged as transformative candidates in solid-state lighting, chemical sensing, anti-counterfeiting, and information encryption due to their millisecond-scale afterglow, high quantum yields, tunable emission profile, and stimuli-responsive phosphorescence switching. These attributes address critical limitations of conventional phosphors—ambient quenching, fixed chromaticity, and poor stimulus adaptivity—through atomically precise triplet-state engineering. The following sections showcase state-of-the-art applications of MOF-based RTP materials *via* representative research.

4.1. Solid-state lighting

White-light-emitting diodes (WLEDs) are cornerstone solid-state lighting technologies with substantial potential for energy savings and carbon-emission mitigation.^{74,75} However, conventional multicomponent routes—phosphor blends or hybrid packages—readily suffer from intrinsic color imbalance, reabsorption losses, and device complexity.⁷⁶ By contrast, single-phase emitters offer spectral stability and enable device miniaturization.⁷⁷ MOF-based RTP phosphors are compelling candidates: their long-lived triplet emission and tunable chromaticity can deliver white light within a single-crystalline, monophasic framework, inherently suppressing phase segregation and supporting stable, efficient illumination for next-generation photonics. For instance, Wang *et al.*⁷⁸ employed one-pot reaction of 15-crown-5 ether with CdX_2 (X = Cl, Br, and I) to obtain three metal-halide MOF hybrids (15-5- $CdCl_2$, 15-5- $CdBr_2$, and 15-5- CdI_2). Under 340 nm excitation, all three emitted near-white light at 298 K with CIE coordinates of

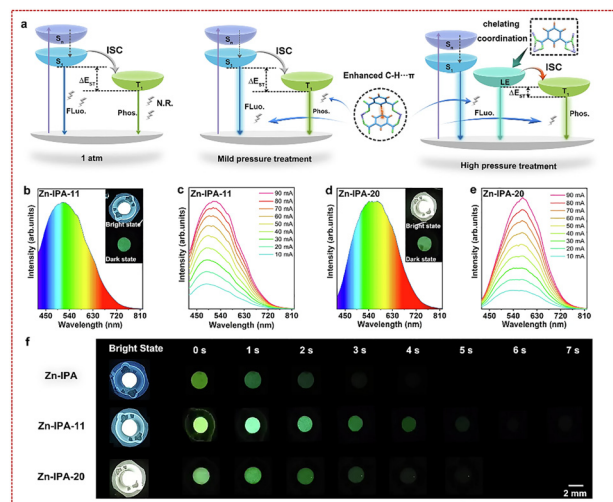


Fig. 9 Pressure-dependent emission mechanisms and applications of Zn-IPA MOFs: (a) Jablonski diagrams for Zn-IPA at ambient pressure and pressure-released states from 11.0 GPa and 20.8 GPa; (b) and (c) emission spectra of Zn-IPA-11 at different operating currents; (d) and (e) emission spectra of Zn-IPA-20 at different operating currents; (f) phosphorescence of pc-LED devices (Zn-IPA series) post-excitation. Reproduced from ref. 79 with permission from Springer Nature, copyright 2025.

(0.28, 0.32), (0.31, 0.39), and (0.30, 0.34), respectively, and displayed excitation-dependent color tuning (blue/cyan \rightarrow green/yellow). Notably, 15-5- $CdCl_2$ and 15-5- $CdBr_2$ showed bright, color-tunable afterglow (1–2 s) attributed to crown-ether confinement that rigidified triplet states and heavy-atom-assisted intersystem crossing. In 2025, Yang *et al.*⁷⁹ reported high-performance white-light emission in Zn-IPA *via* pressure-managed triplet exciton management. At 20.0 MPa, pressure-induced metal–ligand asymmetrical chelate coordination generated an emergent electronic state that narrowed ΔE_{ST} and accelerated intersystem crossing, boosting phosphorescence intensity while modulating singlet/triplet density-of-states (Fig. 9). This yielded broadband white emission (350–800 nm) with a high Φ_{PL} value of 81.3% and CIE coordinates of (0.29, 0.37). Crucially, optimized compression at 11.0 MPa enhanced C–H $\cdots\pi$ rigidification in Zn-IPA-11, synergistically amplifying blue emission and extending a phosphorescence lifetime from 0.91 s to 1.01 s. Fabricated time delay phosphor-converted LEDs exhibited 7 s persistent luminescence post-excitation, demonstrating viable solid-state lighting applications.

4.2. Chemical sensing

Optical sensing provides distinctive advantages, including ultrahigh sensitivity, rapid response kinetics, noninvasive operation, and inherent biocompatibility.⁸⁰ MOF-based RTP systems are particularly compelling due to their exquisite environmental responsiveness—where perturbations selectively modulate singlet/triplet exciton dynamics. This enables precision engineering of stimulus-responsive phosphorescence switching, wherein analyte-gated intensity changes generate quantitative optical readouts for smart sensing platforms.

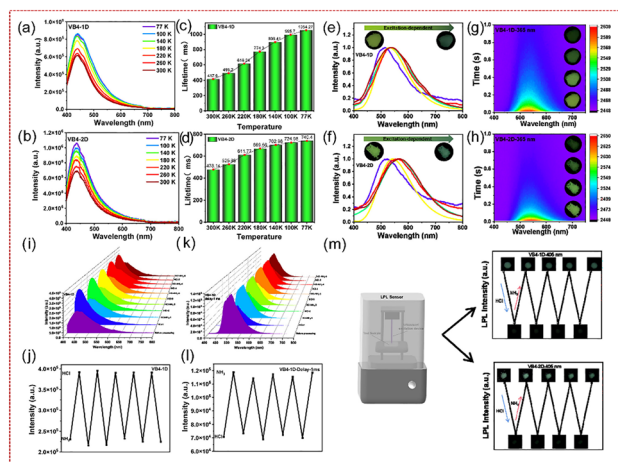


Fig. 10 Stimulus-responsive photophysics of amino-functionalized MOFs: (a) and (b) temperature-dependent emission spectra of VB4-1D and VB4-2D; (c) and (d) temperature-dependent lifetime histogram of VB4-1D and VB4-2D; (e) and (f) delayed spectra of VB4-1D and VB4-2D; (g) and (h) time-dependent delayed spectra and corresponding photographs of VB4-1D and VB4-2D; (i) and (k) fluorescence and time-gated spectra of VB4-1D for HCl and NH₃ fuming for 30 s, respectively; (j) and (l) fluorescence and phosphorescence quenching and recovery upon cycling between HCl and NH₃ fuming; (m) changes in the long persistent luminescence of VB4-1D and VB4-2D before and after fumigation. Reproduced from ref. 27 with permission from American Chemical Society, copyright 2024.

As a paradigm for acid/base optical sensing, Wang *et al.*²⁷ synthesized two amino-decorated MOFs (VB4-2D and VB4-1D) by self-assembling CdCl₂, N-heterocyclic 6-aminopurine, and terephthalic acid. Both displayed excitation-dependent fluorescence and phosphorescence from blue to green and from cyan to green (Fig. 10). Their amino-functionalized porous frameworks enabled analyte-specific interactions, affording a reversible acid/base response. In VB4-1D, HCl vapor (30 s) induced protonation, causing a 25 nm hypsochromic shift from 445 nm to 420 nm with a fluorescence enhancement; subsequent 30 s NH₃ vapor effected deprotonation and fully restored the emission, repeatable over five cycles. Concurrently, the phosphorescence intensity provided an orthogonal channel: HCl quenched the long persistent luminescence by disrupting triplet excitons, whereas NH₃ reinstated it *via* structural reconstruction, yielding a visibly reversible cycle.

In addition, MOF-based RTP platforms have been applied to other important species sensing such as water and antibiotics. For example, Yu *et al.*⁸¹ developed a water-stable 2D lanthanide MOF (NIIC-2-Tb) that detected ultra-selectively ofloxacin *via* luminescence quenching, achieving a detection limit of 1.1×10^{-9} M with a response of 6 s. For real-time monitoring, NIIC-2-Tb was embedded in a carrageenan hydrogel (NIIC-2-Tb@CRG), coupling luminescence transduction with mechanical flexibility to enable on-site visual quantification of ofloxacin residues in meat through stimulus-gated emission switching. In 2025, Mollick *et al.*⁸² engineered polymer/MOF hybrids *via* bottom-up covalent integration, where tunable alkylamine incorporation during synthesis optimized green RTP performance

($\tau_p = 359$ ms at 298 K; 592 ms at 77 K, $\Phi_p = 28\%$). The covalent architecture conferred excellent solution processability, enabling the fabrication of flexible RTP-emitting fibers ($\tau_p = 408$ ms) and films ($\tau_p = 613$ ms at 77 K). These hybrids exhibited pronounced selectivity for water over alcohols, positioning them as versatile candidates for wearable humidity sensors.

4.3. Anti-counterfeiting

MOF-based RTP systems can provide millisecond afterglow, stimulus-gated color switching, and host-guest programmability to create security markers that surpass static anti-counterfeiting technologies.⁵⁸ By exploiting triplet-state dynamics, they enabled naked-eye time-resolved verification, light/solvent/pressure/thermal-triggered chromism, and spatially encoded luminescent patterns—yielding multilevel authentication without specialized equipment.⁸³ In 2023, Gao *et al.*⁵⁴ encapsulated acridine (Ar), pyrene, 9,10-Bis(phenylvinyl) anthracene (BPEA), and coronene in MOFs (DCF-12) to form host-guest hybrids. Pyrene@DCF-12 exhibited excitation-dependent afterglow tunable across 400–620 nm, with color shifting from yellow to orange to red and emission red shifting from 550 to 670 nm (Fig. 11). Under 365 nm irradiation, it showed green emission (518 nm), followed by naked-eye-visible red afterglow ($\tau_p = 340$ ms) persisting >2.5 s post-irradiation, attributed to a reduced S₁(Pyrene)-T₁(host) gap that promoted ISC. For anti-counterfeiting, a tree-trunk pattern was fabricated using phosphorescent Pyrene@DCF-12 (red afterglow) and non-phosphorescent BPEA@DCF-12 (prompt decay). Under 365 nm UV, both showed yellow/green fluorescence; post-UV, only Pyrene@DCF-12 emitted red afterglow. Solvent-gated

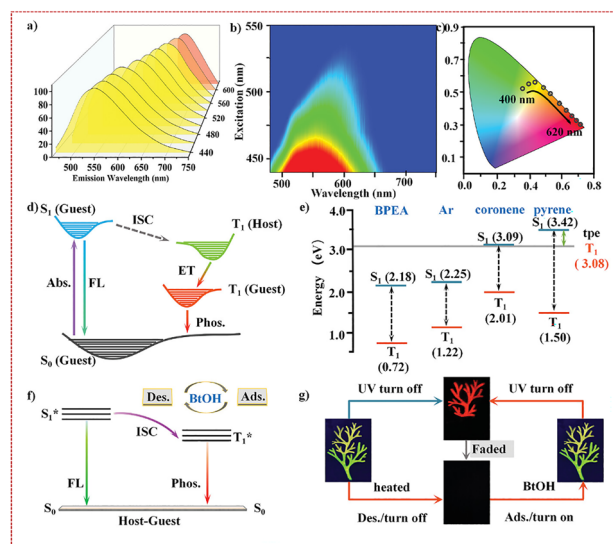


Fig. 11 Photophysical and chiral characteristics of pyrene@DCF-12: (a) excitation-dependent emission spectra; (b) excitation-dependent mapping; (c) CIE chromaticity coordinates at varying excitation wavelengths; (d) proposed guest-to-host energy transfer model; (e) energy level alignment of TPE host and guest emitters; (f) the response mechanism of benzyl alcohol toward phosphorescence; (g) multi-level anti-counterfeiting applications. Reproduced from ref. 54 with permission from Wiley-VCH GmbH, copyright 2023.



Fig. 12 Information encryption with PJJ-1 and PJJ-2: (a) inkjet-printed multicolor security patterns; (b) optical logic gate operation *via* time-resolved anti-counterfeiting system; (c) morse-code dynamic encryption display activated by UV triggering; optical (d) writing and (e) number based on the time-resolved anti-counterfeiting system. Reproduced from ref. 35 with permission from Elsevier, copyright 2025.

reversibility was demonstrated: heating removed benzyl alcohol to quench afterglow, while re-adsorption restored red emission—enabling multi-cycle authentication through vapor-responsive triplet-state switching. Subsequently, Shi *et al.*⁸⁴ established a scalable gram-scale synthesis of high-quality CaL-1 and CaL-2 crystals using 4,5-imidazoledicarboxylic acid, both exhibiting intense RTP at 552 nm and 566 nm with afterglow visible for 13 s. Leveraging this persistent luminescence, they engineered a Python-based dynamic coding algorithm that translates time-resolved phosphorescence patterns into unforgeable security tags. This platform technology was readily extensible to diverse long-persistent luminescent materials for multilevel anti-counterfeiting applications.

4.4. Information encryption

MOF-based RTP materials enable high-security information encryption by harnessing orthogonal stimulus-responsive dimensions: time-gated persistent luminescence creates temporal barcodes decodable *via* delayed detection; excitation-wavelength-dependent emission allows spectral multiplexing within a single material; and host-guest programmable erasure generates transient patterns *via* solvent-induced triplet quenching. These synergistically produce physically unclonable cryptographic functions—demonstrated in Morse-code dynamic displays, logic gates, and self-erasing security inks—where triplet excitons serve as reconfigurable information carriers resistant to physical replication. Wang *et al.*⁸⁵ fabricated MOF-dye gel films that responded to acid/base stimuli. Immersion in artificial sweat (pH 4.7, 20 min) produced distinct chromatic states under 365 nm UV: the left “1” appeared pale red, the center “3” blue, and the right “6” lavender. After UV was switched off, center “3” retained yellow-green phosphorescence, whereas right “6” intensified owing to partial porphyrin protonation. The weak acidity of sweat preserved

residual red fluorescence, keeping “1” legible, while strong acid alone fully quenched emission. This stimulus-gated decryption—where phosphorescence persistence authenticates messages against pH-manipulated decoys—established dual-channel chemical encryption.

Additionally, as a representative case, Wang *et al.*³⁵ engineered two MOFs by self-assembling a charge-transfer ligand (TPP) with lead halides, affording PJJ-1 (PbCl₂) and PJJ-2 (PbCl₂/Br). Under 380 nm excitation, both showed broadband emission, and PJJ-2 delivered cold-white light (CIE: 0.31, 0.46) *via* dual-channel luminescence from both the organic linkers and inorganic secondary building units. Their phosphorescence latency displayed excitation/temperature-dependent chromatic evolution (cyan → green → yellow/orange), enabling temporal barcoding for information encryption. Millisecond-scale lifetime offsets enabled (Fig. 12): (1) 3 × 8 dot matrices using PJJ-2/TPP/PbCl₂ decoded by binary-to-ASCII conversion; (2) time-resolved writing (I/♥/SUST), where “♥SUST” appeared within 1 s, while only “♥” was still visible after >2 s; and (3) multilevel steganography in which a true “7” hidden beneath a decoy “8” was retrievable only after UV cessation >2 s—premature (<2 s) or delayed (>3 s) viewing yielded a false “9” or null output. This self-destructing temporal encryption harnessed MOF-based RTP exciton dynamics for physically unclonable security.

5. Conclusions and outlook

MOF-based RTP has evolved from proof-of-concept emitters to versatile platforms synergizing atomic-precision triplet engineering with programmable host-guest dynamics. Strategic manipulation of metal nodes—particularly closed-shell d¹⁰ centers and halide-rich clusters—combined with heteroatom-enriched ligand architectures (including D-A systems and electron-rich chromophores), guest/solvent programming, and external stimuli collectively satisfy dual RTP requisites: enhanced ISC *via* heavy-atom/charge-transfer mediation and robust triplet stabilization through framework-conferred rigidity. This paradigm has delivered high-efficiency phosphors, single-phase white emitters, LED-activatable persistent luminescence, and intelligent stimulus responses spanning humidity, pressure, and acids/bases. Critically, emergent structure-emission relationships—linking spin-orbit coupling, charge-transfer character, framework topology, and host-guest interactions—now provide crystallographic blueprints for next-generation solid-state lighting, chemical sensing, anti-counterfeiting, and information encryption technologies.

Despite significant advances, MOF-based RTP systems still present key avenues for development. Firstly, deeper mechanistic quantification through multimodal *in situ* spectroscopy and exciton-dynamics simulations is essential to deconvolute the relative roles of LLCT/LMCT/MLCT pathways, host-guest energy/electron transfer, framework rigidification, and O₂/H₂O quenching—thereby enabling the rational design of phosphors with $\Phi_{\text{PL}} > 50\%$ and $\tau_{\text{p}} > 1$ s. Secondly, many high-performing

systems rely on Zn/Cd-containing nodes or high-precision lattices, which hampers device integration and biocompatibility. Efforts should be intensified in key strategies such as covalent polymer-metal-organic framework hybridization, hydrogel encapsulation, printable phosphorescent inks, and additive manufacturing to achieve deviceization while maintaining the crystal integrity and RTP performance. Furthermore, the spectral coverage is largely confined to the visible light region. To extend the emission to the NIR-I/II band (> 800 nm) for meeting the requirements of biological imaging applications, more D-A ligands, lanthanide sensitization, and host-guest energy transfer cascading are required. With atomically precise triplet-state engineering, MOF-based RTP is poised to enable disruptive platforms in solid-state lighting, chemical sensing, anti-counterfeiting, and encryption. Overcoming these challenges will accelerate the transition from laboratory prototypes to industrial technologies.

Conflicts of interest

The authors declare that they have no known competing financial interests for personal relationships that could have appeared to influence the work reported in this paper.

Data availability

No primary research results, software or code have been included and no new data were generated or analysed as part of this review. The data supporting the findings of this review are derived from previously published studies, which have been appropriately cited in the manuscript.

Acknowledgements

This project was supported by the National Key Research and Development Program of China (2023YFB3810001), the NSFC (52333007 and 52273197), the Shenzhen Key Laboratory of Functional Aggregate Materials (ZDSYS2021102111400001), the Science Technology Innovation Commission of Shenzhen Municipality (KQTD20210811090142053 and JCYJ20220818-103007014), the Science and Technology Program of Guangzhou, China (2023A04J0069), the China Postdoctoral Science Foundation (2025M780115), and the Open Fund of the State Key Laboratory of Luminescent Materials and Devices (South China University of Technology).

References

- 1 D. Liu, W. Wang, P. Alam, Z. Yang, K. Wu, L. Zhu, Y. Xiong, S. Chang, Y. Liu, B. Wu, Q. Wu, Z. Qiu, Z. Zhao and B. Tang, Highly efficient circularly polarized near-infrared phosphorescence in both solution and aggregate, *Nat. Photonics*, 2024, **18**, 1276–1286.
- 2 Z. Xu, W. Chen, K. Chen, S. Lin, Z. Wu, G. Deng, J. Chen, M. Tayyab, Y. Xiong, M. D. Li, D. Wang, Z. An and B. Tang, Stimulus-responsive emission via dynamic triplet energy transfer in organic room-temperature phosphorescence glass, *Adv. Mater.*, 2025, **37**, e2418778.
- 3 H. Yang, Y. Wang, X. Yao, H. Ma, J. Yu, X. Li, X. Wang, X. Liang, Q. Peng, S. Cai, Z. An and W. Huang, Efficient and ultralong room temperature phosphorescence from isolated molecules under visible light excitation, *J. Am. Chem. Soc.*, 2025, **147**, 1474–1481.
- 4 J. Ren, M. Gao, Z. Liu, Y. Yang, R. Wu, J. Liang, J. Yang, M. Fang and Z. Li, The impact of molecular packing on organic room temperature phosphorescence and corresponding stimulus response effect, *Adv. Funct. Mater.*, 2024, **34**, 2311659.
- 5 K. Wu, D. Liu, L. Zhu, T. Wu, Y. Xu, C. He, Y. Xiong, Z. Zhao and B. Tang, Recent progress in triplet energy transfer systems toward organic afterglow materials, *Commun. Chem.*, 2025, **8**, 85.
- 6 L. Xiao, Y. Wu, J. Chen, Z. Yu, Y. Liu, J. Yao and H. Fu, Highly efficient room-temperature phosphorescence from halogen-bonding-assisted doped organic crystals, *J. Phys. Chem. A*, 2017, **121**, 8652–8658.
- 7 Y. Wen, H. Liu, S. Zhang, Y. Gao, Y. Yan and B. Yang, One-dimensional π - π stacking induces highly efficient pure organic room-temperature phosphorescence and ternary-emission single-molecule white light, *J. Mater. Chem. C*, 2019, **7**, 12502–12508.
- 8 M. Shimizu, R. Shigitani, M. Nakatani, K. Kuwabara, Y. Miyake, K. Tajima, H. Sakai and T. Hasobe, Siloxy group-induced highly efficient room temperature phosphorescence with long lifetime, *J. Phys. Chem. C*, 2016, **120**, 11631–11639.
- 9 C. Zhou, S. Zhang, Y. Gao, H. Liu, T. Shan, X. Liang, B. Yang and Y. Ma, Ternary emission of fluorescence and dual phosphorescence at room temperature: a single-molecule white light emitter based on pure organic aza-aromatic material, *Adv. Funct. Mater.*, 2018, **28**, 1802407.
- 10 Y. Tao, R. Chen, H. Li, J. Yuan, Y. Wan, H. Jiang, C. Chen, Y. Si, C. Zheng, B. Yang, G. Xing and W. Huang, Resonance-activated spin-flipping for efficient organic ultralong room-temperature phosphorescence, *Adv. Mater.*, 2018, **30**, e1803856.
- 11 W. Huang, B. Chen and G. Zhang, Persistent room-temperature radicals from anionic naphthalimides: spin pairing and supramolecular chemistry, *Chemistry*, 2019, **25**, 12497–12501.
- 12 G. Chen, S. Guo, H. Feng and Z. Qian, Anion-regulated transient and persistent phosphorescence and size-dependent ultralong afterglow of organic ionic crystals, *J. Mater. Chem. C*, 2019, **7**, 14535–14542.
- 13 K. Kanosue, S. Hirata, M. Vacha, R. Augulis, V. Gulbinas, R. Ishige and S. Ando, A colorless semi-aromatic polyimide derived from a sterically hindered bromine-substituted dianhydride exhibiting dual fluorescence and phosphorescence emission, *Mater. Chem. Front.*, 2019, **3**, 39–49.
- 14 B. Wang, Y. Mu, H. Zhang, H. Shi, G. Chen, Y. Yu, Z. Yang, J. Li and J. Yu, Red room-temperature phosphorescence of

- CDs@Zeolite composites triggered by heteroatoms in zeolite frameworks, *ACS Cent. Sci.*, 2019, **5**, 349–356.
- 15 Z. Lv, R. Lin, Y. Yang, K. Lan, C. T. Hung, P. Zhang, J. Wang, W. Zhou, Z. Zhao, Z. Wang, J. Zou, T. Wang, T. Zhao, Y. Xu, D. Chao, W. Tan, B. Yan, Q. Li, D. Zhao and X. Li, Uniform single-crystal mesoporous metal-organic frameworks, *Nat. Chem.*, 2025, **17**, 177–185.
 - 16 X. Yang and D. Yan, Long-afterglow metal-organic frameworks: reversible guest-induced phosphorescence tunability, *Chem. Sci.*, 2016, **7**, 4519–4526.
 - 17 D. Li, X. Yang and D. Yan, Cluster-based metal-organic frameworks: modulated singlet-triplet excited states and temperature-responsive phosphorescent switch, *ACS Appl. Mater. Interfaces*, 2018, **10**, 34377–34384.
 - 18 X. Yang and D. Yan, Strongly enhanced long-lived persistent room temperature phosphorescence based on the formation of metal-organic hybrids, *Adv. Opt. Mater.*, 2016, **4**, 897–905.
 - 19 Y. J. Ma, X. Fang, G. Xiao and D. Yan, Dynamic manipulating space-resolved persistent luminescence in core-shell MOFs heterostructures via reversible photochromism, *Angew. Chem., Int. Ed.*, 2022, **61**, e202114100.
 - 20 B. Xu, Z. F. Wang, J. Shen, J. Li, Y. H. Jia, T. L. Jiang, Z. H. Gao, X. Wang and X. E. Meng, Metal-organic framework-activated full-color room-temperature phosphorescent carbon dots with a wide range of tunable lifetimes for 4D coding applications, *J. Phys. Chem. C*, 2022, **126**, 11701–11708.
 - 21 J. Oh, S. Lee, H. Han, O. Allam, J. Choi, H. Lee, W. Jiang, J. Jang, G. Kim, S. Mun, K. Lee, Y. Kim, J. Park, S. Lee, S. Jang and C. Park, Dual-light emitting 3D encryption with printable fluorescent-phosphorescent metal-organic frameworks, *Light: Sci. Appl.*, 2023, **12**, 226.
 - 22 Q. Yu, H. Sung, F. Gao, I. Williams, J. Lam, J. Sun and B. Tang, Ligand meta-anchoring strategy in metal-organic frameworks for remarkable promotion of quantum yields, *Angew. Chem., Int. Ed.*, 2024, **63**, e202401261.
 - 23 D. Briones, P. Leo, J. Cepeda, G. Orcajo, G. Calleja, R. Sanz, A. Rodríguez-Diéguez and F. Martínez, Alkaline-earth metal based MOFs with second scale long-lasting phosphor behavior, *CrystEngComm*, 2018, **20**, 4793–4803.
 - 24 H. Liu, W. Ye, Y. Mu, H. Ma, A. Lv, S. Han, H. Shi, J. Li, Z. An, G. Wang and W. Huang, Highly efficient blue phosphorescence from pillar-layer MOFs by ligand functionalization, *Adv. Mater.*, 2022, **34**, e2107612.
 - 25 B. Zhou, Z. Qi and D. Yan, Highly efficient and direct ultralong all-phosphorescence from metal-organic framework photonic glasses, *Angew. Chem., Int. Ed.*, 2022, **61**, e202208735.
 - 26 H. Sun, Z. Wang, R. Huang, Z. Chen and M. Pan, Reversible multilevel stimuli-responsiveness and multicolor room temperature phosphorescence to fluorescence transition based on a metal-organic framework system, *Chem. Eng. J.*, 2025, **506**, 160075.
 - 27 Z. Wang, X. Chen, D. Wang, Y. Zhou, M. Li and J. Mo, Reversible acid-base long persistent luminescence switch based on amino-functionalized metal-organic frameworks, *Inorg. Chem.*, 2024, **63**, 1188–1196.
 - 28 D. Yang, H. Zheng, Y. Fang, Q. Liang, Q. Han, Y. Shi and X. Zheng, Multistimuli-responsive materials based on Zn(II)-viologen coordination polymers and their applications in inkless print and anticounterfeiting, *Inorg. Chem.*, 2022, **61**, 7513–7522.
 - 29 B. Zhou and D. Yan, Long persistent luminescence from metal-organic compounds: state of the art, *Adv. Funct. Mater.*, 2023, **33**, 2300735.
 - 30 Q. Wu, X. Gao, W. Zhang and Y. Wang, Molecular engineering of ionic metal-organic frameworks via ligand conjugation modulation for tailored phosphorescence and multilevel encryption, *Adv. Sci.*, 2025, e09013.
 - 31 K. Zhang, N. Dan, R. Zhang, J. Wei, R. Tian, Y. Zhang, H. Fu, M. Qiu, L. Ma and S. Zang, Multi-stimuli-responsive circularly polarized luminescence with handedness inversion and near-infrared phosphorescence in chiral metal-organic framework platform for white light emission and information encryption, *Adv. Sci.*, 2025, **12**, e2502784.
 - 32 Q. Yu, J. Zhang, J. Lam, D. Yang, J. Sun and B. Tang, Tunable room temperature phosphorescence in heavy-atom-free metal-organic frameworks by ligand functionalization, *ACS Mater. Lett.*, 2023, **5**, 2691–2699.
 - 33 L. Geng, K. Wang, R. Sun, C. Li, X. Li, M. Zhang, M. Yu, Z. Chang and X. Bu, Donor-acceptor metal-organic frameworks featuring tunable triplet states for multistimulus responsive room-temperature charge transfer phosphorescence, *CCS Chem.*, 2025, **7**, 416–428.
 - 34 M. Gutiérrez, C. Martín, J. Hofkens and J. Tan, Long-lived highly emissive MOFs as potential candidates for multiphotonic applications, *J. Mater. Chem. C*, 2021, **9**, 15463–15469.
 - 35 Z. Wang, J. Pan, X.-Q. Chen, M. Li and M. Pan, Multi-color long persistent luminescence in metal-organic frameworks regulated by dual channels of distorted second building units and organic ligand and applied in printing, message encryption and writing, *Chem. Eng. J.*, 2025, **509**, 161076.
 - 36 X. Yang, X. Lu, Z. Zhai, J. Qin, X. Chang, M. Han, F. Li and L. Ma, π -Type halogen bonding enhanced the long-lasting room temperature phosphorescence of Zn(ii) coordination polymers for photoelectron response applications, *Inorg. Chem. Front.*, 2020, **7**, 2224–2230.
 - 37 J. Yuan, J. Dong, S. Lei and W. Hu, Long afterglow MOFs: a frontier study on synthesis and applications, *Mater. Chem. Front.*, 2021, **5**, 6824–6849.
 - 38 X. Li, Y. Wang, Z. Zhang, S. Cai, Z. An and W. Huang, Recent advances in room-temperature phosphorescence metal-organic hybrids: structures, properties, and applications, *Adv. Mater.*, 2024, **36**, 2308290.
 - 39 Y. Zhu, X. Wang and M. Wu, Intriguing room temperature phosphorescence in crystalline porous organic frameworks, *Adv. Funct. Mater.*, 2023, **33**, 2308096.
 - 40 X. Lu, K. Zhang, X. Niu, D. Ren, Z. Zhou, L. Dang, H. Fu, C. Tan, L. Ma and S. Zang, Encapsulation engineering of porous crystalline frameworks for delayed luminescence

- and circularly polarized luminescence, *Chem. Soc. Rev.*, 2024, **53**, 6694–6734.
- 41 H. Wu, X. Lu, J. Chen, X. Yang, W. Qin and L. Ma, Long afterglow of a nonporous coordination polymer with tunable room-temperature phosphorescence by the doping of dye molecules, *Inorg. Chem.*, 2021, **60**, 846–851.
- 42 D. Lu, Z. Wang, F. Wang and J. Zhang, Phosphorescent calcium-based metal-organic framework with second-scale long afterglow, *Inorg. Chem.*, 2021, **60**, 10075–10078.
- 43 W. Lv, Y. Ma, A. Wang, Y. Mu, S. Niu, L. Wei, W. Dong, X. Ding, Y. Qiang, X. Li and G. M. Wang, Al₈ cluster-based metal halide frameworks: balancing singlet-triplet excited states to achieve white light and multicolor luminescence, *Small*, 2024, **20**, e2306713.
- 44 Z. Wang, J. Liu, M. Li and G. Chen, White light and long persistent luminescence from metal cluster-based metal-organic frameworks, *Chem. Eng. J.*, 2023, **462**, 142154.
- 45 T. Chen, Y. J. Ma, G. Xiao, X. Fang, Y. Liu, K. Li and D. Yan, The trade-off anionic modulation in metal-organic glasses showing color-tunable persistent luminescence, *Mater. Horizons*, 2024, **11**, 4951–4960.
- 46 Z. Long, Y. Wu, Y. Zheng, R. Shi and D. Lu, Room-temperature phosphorescence of a calcium-based metal-organic framework, *Mater. Lett.*, 2024, **357**, 135753.
- 47 Y. Jiang, K. Zhang, M. Zhou, P. Gao and H. Fu, A fluorescence/phosphorescence dual-emitting metal-organic framework exhibiting two approaches for single-phase white-light emission, *J. Solid State Chem.*, 2021, **304**, 135753.
- 48 Z. Wang, C. Zhu, Z. Wei, Y. Fan and M. Pan, Breathing-ignited long persistent luminescence in a resilient metal-organic framework, *Chem. Mater.*, 2020, **32**, 841–848.
- 49 J. Ma, R. Feng, Y. Jia, M. Zhang and S. Guo, Li, Na, and Cs-based metal-organic frameworks for room temperature phosphorescence applications, *Sci. China Chem.*, 2025, **68**, 3019–3027.
- 50 X. Chen, S. Wang, M. An, Z. Chen and Z. Wang, Old bottles of new wines: dynamic multimode color-tuning long afterglow and white light emission in cost-effective metal-organic frameworks (MOFs), *ACS Mater. Lett.*, 2025, **7**, 417–424.
- 51 H. Mieno, R. Kabe, N. Notsuka, M. D. Allendorf and C. Adachi, Long-lived room-temperature phosphorescence of coronene in zeolitic imidazolate framework ZIF-8, *Adv. Opt. Mater.*, 2016, **4**, 1015–1021.
- 52 T. Zhao, D. Busko, B. Richards and I. Howard, Limitation of room temperature phosphorescence efficiency in metal organic frameworks due to triplet-triplet annihilation, *Front. Chem.*, 2022, **10**, 1010857.
- 53 T. Xiao, Y. Shi, D. Yang, H. Zheng, Y. Fang, Q. Liang and X. Zheng, A UV and X-ray dual photochromic Zn (II) metal-organic framework based on viologen: Photo-controlled luminescence and temperature-dependent phosphorescence, *Dyes Pigm.*, 2022, **208**, 110812.
- 54 P. Gao, K. Zhang, D. Ren, H. Liu, H. Zhang, H. Fu, L. Ma and D. Li, Host-guest chemistry of chiral mofs for multi-color circularly polarized luminescence including room temperature phosphorescence, *Adv. Funct. Mater.*, 2023, **33**, 2300105.
- 55 A. Ni, B. Zhang, P. Zhang, J. Zhang, H. Wang, K. Feng, S. Liu, J. Ni and C. Duan, Water friendly room temperature phosphorescence doped materials prepared via metal organic framework matrix transformation, *Dyes Pigm.*, 2023, **210**, 110959.
- 56 P. Liao, J. Liu, H. Fan, Y. Ding and M. Tong, Dual functionality of phosphorescence and photothermal conversion through light-activated open-shell singlet diradicals in silver metal-organic frameworks, *J. Mater. Chem. C*, 2025, **13**, 16712–16721.
- 57 J. Chen, R. Sun, W. Yang, F. Xing, X. Yu and L. Sun, Europium ions modulated room temperature phosphorescence in dye-encapsulated MOFs for dual-modal fluorescence-afterglow, *J. Mater. Chem. C*, 2025, **13**, 1157–1164.
- 58 J. Liu, Y. Zhuang, L. Wang, T. Zhou, N. Hirotsuki and R. J. Xie, Achieving multicolor long-lived luminescence in dye-encapsulated metal-organic frameworks and its application to anticounterfeiting stamps, *ACS Appl. Mater. Interfaces*, 2018, **10**, 1802–1809.
- 59 H. Zhang, Y. Yan, G. Qiao and J. Li, Multi-emissive room temperature phosphorescence of a two-dimensional metal-organic framework, *Inorg. Chem. Commun.*, 2019, **104**, 119–123.
- 60 Z. Zhao, J. Ru, P. Zhou, Y. Wang, C. Shan, X. Yang, J. Cao, W. Liu, H. Guo and Y. Tang, A smart nanoprobe based on a gadolinium complex encapsulated by ZIF-8 with enhanced room temperature phosphorescence for synchronous oxygen sensing and photodynamic therapy, *Dalton Trans.*, 2019, **48**, 16952–16960.
- 61 X. Yang, Z. Zhai, X. Lu, J. Qin, F. Li and L. Ma, Hexanuclear Zn(II)-induced dense pi-stacking in a metal-organic framework featuring long-lasting room temperature phosphorescence, *Inorg. Chem.*, 2020, **59**, 10395–10399.
- 62 D. Zhang, J. Hu, Y. Zhu, M. Wang, J. Liu, H. Li, T. Li, Z. Liu, J. Li and W. Zhang, Constructing low-dimensional phosphorescent MOFs by site-selective coordination engineering, *J. Mol. Struct.*, 2025, **1334**, 141861.
- 63 J. Mo, Z. Wang, X. Xu, F. Dieter, M. Pan and C. Su, Bright long persistent luminescence in cluster-based MOFs derived from intra-ligand charge transfer characteristic, *Chem. Eng. J.*, 2024, **483**, 141861.
- 64 R. Li, M. Shi, R. Tian, Q. Gao, Z. Liu, G. Chen, T. Zhao, B. Lu and F. Peng, Facile preparation of full-color room temperature phosphorescence metal-organic framework via covalent ligand decoration, *J. Colloid Interface Sci.*, 2025, **687**, 345–352.
- 65 X. Xue, S. Wang, M. Li and Z. Wang, Ultralong room-temperature phosphorescence in ca(ii) metal-organic frameworks based on nicotinic acid ligands, *Inorg. Chem.*, 2024, **63**, 21336–21344.
- 66 Z. Wang, J. Liu, S. Yin, M. Li, Y. J. Hou, D. Wang, J. Mo and G. Chen, Ultralong near infrared room temperature phosphorescence in Cu(I) metal-organic framework based-on D-π-A-π-D linkers, *Adv. Funct. Mater.*, 2023, **33**, 2212985.

- 67 M. Zheng, Z. Jin, Z. Ma, Z. Gu and J. Zhang, Photo-curable 3d printing of circularly polarized afterglow metal-organic framework monoliths, *Adv. Mater.*, 2024, **36**, e2313749.
- 68 Q. Yu, Z. Deng, R. Chen, J. Zhang, R. Kwok, J. Lam, J. Sun and B. Tang, Ligand-to-ligand charge transfer induced red-shifted room temperature phosphorescence in metal-organic frameworks, *J. Am. Chem. Soc.*, 2025, **147**, 10530–10539.
- 69 J. Mo, X. Chen, S. Wang, J. Pan, M. Li and Z. Wang, Broadly excited red long persistent luminescence from hetero-ligand MOFs, *Dalton Trans.*, 2025, **54**, 5859–5867.
- 70 W. Zhang, B. Zhang, T. Wang, J. Chen, Z. Li, R. Wang, S. Liu and J. Zhang, Two new Cd-based metal-organic frameworks for afterglow detection of Fe^{3+} and NH_3 , *J. Mater. Chem. A*, 2024, **12**, 7732–7741.
- 71 S. Liu, Y. Lin and D. Yan, Dynamic multi-color long-afterglow and cold-warm white light through phosphorescence resonance energy transfer in host-guest metal-organic frameworks, *Sci. China Chem.*, 2023, **66**, 3532–3538.
- 72 Q. Niu, Z. Ge, X. Liu, T. Guo, Z. Hu, W. Li and Z. Li, Reversible regulation of room temperature phosphorescence and fluorescence in cucurbit[8]uril-mediated lanthanide MOFs, *Chem. Eng. J.*, 2025, **517**, 164465.
- 73 H. Sun, Q. Zhang, Z. Wang, Y. Huang and M. Pan, Transformational modulation of fluorescence to room temperature phosphorescence in metal-organic frameworks with flexible c–s–c bonds, *ACS Appl. Mater. Interfaces*, 2024, **16**, 11730–11739.
- 74 Y. Sun, K. Wang, X. Huang, S. Wei, E. Contreras, P. Jain, L. M. Campos, H. Kulik and J. S. Moore, Caged aiegens: multicolor and white emission triggered by mechanical activation, *J. Am. Chem. Soc.*, 2024, **146**, 27117–27126.
- 75 Y. Wang, F. Zhang, Z. Qi, X. Zhao, N. Zhang, H. Li, H. Li and X. M. Zhang, Photochemical synthesis of $\text{Ag}_{12}\text{Cu}_7$ nanocluster with cuprophilicity-related long-lived phosphorescence, *Aggregate*, 2024, **6**, e675.
- 76 B. Zhang, L. Miao, W. Song, J. Zhang, J. Chen, T. Wang, W. Zhang, J. Ni and Z. Zhao, Precisely regulating photo-activated dynamic room temperature phosphorescence by alkyl chain-induced lattice-softening, *Adv. Funct. Mater.*, 2024, **35**, 2415094.
- 77 B. Zhou and D. Yan, Glassy inorganic-organic hybrid materials for photonic applications, *Matter*, 2024, **7**, 1950–1976.
- 78 Z. Wang, J. T. Mo, J. J. Pan and M. Pan, White light and color-tuning long persistent luminescence from metal halide based metal-organic frameworks, *Adv. Funct. Mater.*, 2023, **33**, 2300021.
- 79 Q. Yang, W. Wang, Y. Yang, P. Li, X. Yang, F. Bai and B. Zou, Pressure treatment enables white-light emission in Zn-IPA MOF via asymmetrical metal-ligand chelate coordination, *Nat. Commun.*, 2025, **16**, 696.
- 80 X. Zhang, X. Yi, J. Ouyang, S. Wang, D. Xu, X. Qi, P. Jiang, X. Guo and Y. Wu, Chitosan/carbon dots-loaded nanocellulose/layered double hydroxides composite hydrogel for effective detection and removal of iodide ion, *Chem. Eng. J.*, 2024, **479**, 147753.
- 81 X. Yu, A. Ryadun, D. Pavlov, T. Guselnikova, A. Potapov and V. Fedin, Ln-MOF-based hydrogel films with tunable luminescence and afterglow behavior for visual detection of ofloxacin and anti-counterfeiting applications, *Adv. Mater.*, 2024, **36**, e2311939.
- 82 S. Mollick, V. Kachwal, B. Hupp, Y. D. More, M. Tricarico, A. Steffen and J. Tan, Modulating ultralong room-temperature phosphorescence through mechanical confinement of tailored polymer/MOF hybrid interfaces, *Chem. Sci.*, 2025, **16**, 15185–15193.
- 83 H. Zheng, Q. Wang, X. Wang, F. Wang, S. Li and J. Zhang, Dual-ligand chiral MOFs exhibiting circularly polarized room temperature phosphorescence for anti-counterfeiting, *Sci. China Chem.*, 2025, **68**, 3064–3070.
- 84 R. Shi, Z. Long, F. Wang, L. Gong, X. Lin, G. Zhuang and D. Lu, Two calcium-based metal organic frameworks with long afterglow as anticounterfeiting materials, *Chem. Eng. J.*, 2024, **479**, 147851.
- 85 X. Wang, H. Zhang, J. Li and G. Zou, Monitoring of sweat pH and dual-mode anti-counterfeiting from metal-organic framework-based multifunctional gel, *Chin. J. Chem.*, 2023, **42**, 491–498.